Experimental study of colloidal aggregation in two dimensions. I. Structural aspects

D.J. Robinson and J.C. Earnshaw
The Department of Pure and Applied Physics, The Queen's University of Belfast, Belfast BT7 1NN, Northern Ireland
(Received 16 January 1992)

The morphology of structures formed during the two-dimensional aggregation of colloidal particles at a liquid surface has been studied. The aggregation was induced by adding $CaCl_2$ solution to the aqueous subphase, the electrolyte concentration being varied to change the growth conditions. Under all conditions the clusters displayed self-similarity, the fractal dimension D determined by three independent methods concurring. For low subphase molarities the measured values of D were in accord with predictions for reaction-limited cluster-cluster aggregation, whereas at high molarities D agreed well with expectation for the diffusion-limited case. The cluster anisotropy was greater in the former regime than in the latter, again in accord with theoretical expectation. The change from one regime to the other occurred over a rather narrow range of electrolyte concentration.

PACS number(s): 68.70.+w, 82.70.Dd

I. INTRODUCTION

The study of the aggregation of colloids has a long history, but has undergone a recent resurgence, stimulated by the recognition of the fractal character of the aggregates, which has permitted the quantitative investigation of the disordered structures formed. In many cases the clusters present at all stages of the aggregation process are mobile and may adhere to each other on contact. Such cases can be described as cluster-cluster aggregation [1, 2], and may be contrasted with other processes such as particle-cluster aggregation [3], in which only monomers diffuse, adhering to a selected cluster. Two limiting regimes have been demonstrated by computer simulation [1, 4], which may be compared to "rapid" and "slow" aggregation in the classical literature. The first, governed purely by the diffusive motion of the clusters, which stick on first contact, is referred to as diffusion-limited cluster aggregation (DLCA). The second occurs when the probability of two clusters sticking is low, so that many contacts can be explored before clusters finally adhere: the so-called chemically or reaction-limited case (RLCA).

The process is statistical and appears independent of the exact nature of colloidal particle or interaction involved—it is universal [5]. Recent studies [6] suggest that the kinetics of the aggregation process and the behavior of the distribution of cluster masses are intimately related to cluster structure. To completely characterize the aggregation regime in an experimental situation, it does not suffice to determine the structure of the clusters: the aggregation kinetics and cluster mass distribution must also be studied.

The present series of papers concerns aggregation in a two-dimensional system. Apart from the inherent interest of low-dimensional systems, the study of aggregation in two rather than three dimensions presents certain advantages. Sedimentation of large aggregates does not pose a problem; visualization of the structure is more straightforward, problems due to projection into two-dimensional images being obviated; the high density limit of cluster-cluster aggregation can be realized and studied more easily; and finally, the aggregates are less liable to mechanical instability induced by bending or hydrodynamic stress. It is often possible to image individual particles, providing a direct comparison with computer simulations. We have therefore undertaken a comprehensive investigation of colloidal aggregation in two dimensions. The present paper is restricted to the structural aspects of this aggregation, while the kinetic aspects are treated in the following paper [7] (hereafter referred to as paper II). A third paper [8] (paper III) seeks to resolve apparent conflicts in the conclusions drawn in the first two.

Colloidal particles can be trapped at a liquid surface by surface tension [9] and electrostatic forces [10]. Monolayers of such particles are widespread, appearing in such diverse technological fields as enhanced oil recovery [11], detergency [12], and food manufacture [13]. They provide an experimentally convenient approach to a two-dimensional system, in which, in principle, the interparticle interactions can be modified to cause either DLCA or RLCA.

This paper presents data on the structural properties of aggregates in such systems. The fractal dimension of the colloidal aggregates and its variation with experimental conditions have been determined. This provides only a partial characterization of the structural information embodied in the aggregates, so we have also determined the intrinsic anisotropy of the structures, reflecting departures from spherical symmetry.

A number of previous studies of cluster structure in two-dimensional aggregation have been reported [14–19]. Most, but not all, have involved colloidal particles dispersed at a liquid surface, aggregation being induced by adding electrolyte to the liquid. This reduces the repulsive electrostatic forces, allowing the particles to approach sufficiently close that van der Waals attraction can cause adhesion. In such circumstances cluster-cluster aggregation would be expected. Most of these studies

only considered the cluster self-similarity, and there appears to have been only one brief report of the experimental determination of cluster anisotropy, in shear-induced aggregation [20].

While some studies [17, 18] have found self-similar structure such as expected for DLCA in two dimensions ($D = 1.44 \pm 0.04$), others have quoted fractal dimensions which differ significantly from those expected for either DLCA or RLCA [14–17]. Various modifications of the basic models have been proposed to account for the discrepancies. Thus D may increase to 1.75 ± 0.07 for DLCA in a system of high initial particle density as the system approaches the sol-gel transition [21], agreeing with certain experimental results [14, 15, 17]. Similarly, variants on DLCA invoked to account for the effects of electrostatic polarization of the clusters can produce D as low as 1.26 ± 0.06 in two dimensions [22], resembling other results [16]. In none of these experiments was the variation of D with electrolyte concentration investigated.

II. EXPERIMENTAL METHODS

The colloidal particles used were sulfonated polystyrene latex spheres of nominal diameter 1.088 ± 0.079 μm (Seragen Diagnostics Ltd.). The comparatively low surface concentration of acid groups implies that aggregation of these particles should be more easily induced by addition of electrolyte than for other types. This is a major consideration for surface colloidal work, for which a larger electrolyte concentration is required to screen the particle charge than for bulk colloidal suspensions [16]. The latex was stripped of all water soluble ions and adsorbed surfactants by cleaning with mixed-bed ion exchange resin, which also converted the acid groups on the particles to the hydrogen form. After this treatment most samples remained stable to autoflocculation. Conductiometric titration yielded a surface charge density of 4.0 ± 0.4 μC/cm^2 for the treated particles.

After ion exchange treatment the particles were resuspended in methanol. Colloidal monolayers were formed by dispensing a measured volume of this suspension onto a 5-mm-deep $0.001M$ aqueous NaCl subphase (water from a Millipore Milli-Q system). The methanol dispersed the particles across the surface and rapidly evaporated, leaving them as a colloidal monolayer on the surface. It was found that the slightly salty subphase led to more uniform spreading of the colloidal monolayer. With care it was possible to form very homogeneous monolayers in this way. The monolayers were stable against aggregation on the NaCl subphase for at least 48 h. There was negligible penetration of methanol into the bulk fluid; the substrate tension and viscosity did not change when the spreading protocol was followed using methanol alone.

Aggregation was induced by introduction of a strong electrolyte solution into the subphase through a hydrophobic (Teflon) needle. The electrolyte solution, in volume roughly equal to that of the original subphase, was gently introduced over about 10 min (using an infusion pump) into the subphase, where, being denser, it sank to the bottom of the cell. Divalent $CaCl_2$ was preferred as the electrolyte because it did not crystallize out of solution, as did NaCl. In preliminary experiments [23] the kinetics were considerably different to those expected. This was found to be due to the time required for the denser $CaCl_2$ solution to reach the aqueous surface by diffusive mixing. Various stratagems were adopted to overcome this problem. However, it was found that these did not affect the structural aspects of the aggregates studied here, and so details are deferred to paper II.

The subphase was contained in a simple glass cell, 50×50 mm^2 by 7 mm deep. The cell was placed on an inverted microscope with a long working distance condenser to permit a perspex enclosure to surround the cell for environmental control. A video camera was used to record video images which were subsequently acquired for analysis by a frame grabber. With a $10\times$ objective the magnification was found to be 95 pixels to 100 μm of the image, with less than 2% distortion in all directions across the entire field of view. The surface concentration of the colloid varied somewhat, typically being 8%, there being some 3×10^4 particles in the field of view.

The video images were sharpened to remove noise and rescaled relative to a threshold level to yield binary values. The choice of threshold was not critical: because of the sharpness of the images, any level within a range of about 10 of the original 256 grey levels did not markedly alter the final image. The digitized and rescaled images were systematically scanned to identify sets of adjoining pixels ("clusters"). Clusters intersecting the boundary of the image were rejected, avoiding some potential biases.

III. THEORETICAL BACKGROUND

Several different forces act on interfacial colloidal particles. Some, such as that due to capillarity-induced surface dimpling, are much too small (depth of dimple at the contact line $\sim 10^{-7}$ of a particle radius) to play any significant role for individual 1-μm particles [24], and can be neglected in the present work. Colloidal particles bear electrostatic charges on their wetted portions, which, together with the Debye cloud of counterions, constitute electric dipoles when the particles are at a liquid interface. The force between such dipoles is a r^{-3} repulsion [25]. At smaller distances the attractive van der Waals forces take over. There may be steric effects or other specifically surface forces, but for the present it will suffice to consider these two contributions.

It is possible to systematically modify the balance between these forces, and hence the barrier to aggregation. By adding electrolyte to the subphase the Debye screening length can be reduced to such small magnitudes that the van der Waals attraction can dominate. At low electrolyte concentration the dipole-dipole repulsion will still be present, albeit reduced in strength, so one might anticipate a low probability of sufficiently close approach of two clusters to permit sticking, whereas at higher concentrations the screening would be more effective so that a sticking probability closer to unity might be appropriate.

A. Cluster self-similarity

While the self-similarity of deterministic fractals is readily apparent, that of natural or random structures is less evident, being statistical in nature. It is not obvious that a unique value can be attached to the fractal dimension of such structures. Indeed it seems probable that different weightings implicit in various definitions which can be used may lead to different numerical estimates [26]. We have, therefore, applied three different algorithms to determine the fractal dimensions of the observed clusters. Apart from the basic scaling relations and definitions used, a few details of the implementation of these algorithms will be given at this point.

In the present experiments digitized video images were analyzed. It is then convenient to express lengths and cluster mass in pixels. The pixels, which were ~ 1 μm square, closely approximated the colloidal particles, which were nominally of 1 μm diameter. In all calculations particle positions have thus been replaced by pixel coordinates.

To illustrate the scale invariant nature of the aggregates we consider the scaling law between their mass and their size:

$$M \propto R_g^D, \tag{1}$$

where R_g is the radius of gyration. The inertia tensor of a system of s particles in a space of dimension d spanned by coordinate axes a and b ($a, b \leq d$, here 2) is

$$(R_{ab})^2 = \frac{1}{s} \sum_{i,j=1}^{s} (r_{ia} - r_{ja})(r_{ib} - r_{jb}), \tag{2}$$

where i and j label the individual particles in the cluster. Diagonalization of this tensor yields the principle radii of gyration. For a two-dimensional lamella R_g is the trace of the diagonalized tensor. Equation (1) assumes that in the asymptotic limit R_g is linearly proportional to the total cluster size and that corrections due to cluster boundary effects can be neglected.

A second method (nested squares) considers the mass within a given partition of the cluster. The number of particles lying within a box, of side l and centered near the cluster centroid, should scale as

$$N_b(l) \propto l^D. \tag{3}$$

For uniform fractals whose mass distribution shows no multifractal spectrum the scaling observed by dilating a box centered on a given point is equivalent to that found by covering the structures with a lattice of boxes [27]. [A similar caveat applies to the use of Eq. (1).] It has been suggested that this method yields a slightly smaller estimate of D than the radius of gyration method [28, 29].

In implementing the second method some caution was needed. First, a square box, with an odd number of pixels on a side, avoided practical difficulties in determining whether a pixel fell within a circular box. Second, arbitrariness in the choice of origin may lead to breakdown of scaling. In some previous studies [30] the center of the box of side l was relocated to coincide with the centroid of those particles within the box: here we averaged $N_b(l)$ computed for boxes centered on that pixel closest to the centroid of the cluster and on each of the eight adjacent pixels.

A third method probes scale invariance of the internal structure of the clusters. It is based on the density-density correlation function $C(r)$:

$$C(r) = \frac{1}{s} \sum_{\mathbf{r}} \rho(\mathbf{r} + \mathbf{r}')\rho(\mathbf{r}'), \tag{4}$$

where $\rho(\mathbf{r})$ is the local density, representing the probability (0 or 1) that there is a particle at $\mathbf{r}$. The pixel closest to the centroid of each aggregate was chosen as the origin $\mathbf{r}'$, and to avoid edge effects the range of r was restricted to the smaller of the two linear dimensions of the cluster, relative to $\mathbf{r}'$. For self-similar, spherically symmetric clusters the correlation function decays as

$$C(r) \propto r^{D-d}, \tag{5}$$

reflecting the fractal dimension D. The intrinsic anisotropy of clusters formed by cluster-cluster aggregation should not affect $C(r)$ provided that the data are averaged over many clusters randomly oriented in space.

It is not obvious that these methods will yield concurrent estimates of D. For example, the radius of gyration method weights more distant parts of the structures more heavily [effective r^2 weighting in Eq. (2)]. There seems no general answer to this problem: it must be considered on a case-by-case basis [26]. Strictly each value of D should be identified separately. As they appear to agree for the present data we will simply speak of *the* fractal dimension.

All three algorithms were tested on deterministic images to demonstrate the correctness of coding and to gain some understanding of their limitations as applied to real structures. The only effects which might be relevant related to cluster polydispersity. For polydisperse test images some correlations were evident in the residuals of power-law fits to $N_b(l)$ vs l and $C(r)$ vs r, limiting the useful scaling range.

B. Cluster anisotropy

The fractal dimension, often the sole structural parameter used in aggregation studies, may not suffice to uniquely characterize the morphology of random aggregates. While D may well reflect much of the available structural information for spherically symmetric structures, this is not so for cluster-cluster aggregation, where the structures lose spherical symmetry. A tenuous but spherically symmetric structure could have the same fractal dimension as a more compact but linear structure; they can, however, be separated by their anisotropy.

The anisotropy can be defined in terms of the sequence of principal radii of gyration R_i^2, ranked in order of decreasing magnitude: $R_1^2 \geq R_2^2 \geq \cdots \geq R_d^2$, as

$$A = \frac{R_1^2}{R_d^2}. \tag{6}$$

TABLE I. Theoretical predictions of structural parameters of aggregates: D [29] and A [31]. (Fractional errors for A' should be the same as for A.)

	DLCA	RLCA
D	1.44 ± 0.04	1.55 ± 0.03
A	5.7 ± 0.2	4.7 ± 0.2
A'	4.4	3.6

Botet and Jullien [31] have estimated the anisotropy thus defined from numerical simulations. Two different values can be computed: the ratio of the averages of the principal radii of gyrations, $A = \langle R_1^2 \rangle / \langle R_2^2 \rangle$ in two dimensions, and the alternative average of the ratio [31], $A' = \langle R_1^2 / R_2^2 \rangle$. As expected, these are different, A' being 23% less than A.

C. Summary

The fractal dimension and anisotropy of aggregates formed in two-dimensional systems are significantly different for the two main cluster-cluster aggregation models, DLCA and RLCA. Results from simulations are summarized in Table I. The data from our experimental study will be compared to these predictions.

IV. RESULTS

Experiments were carried out over a range of surface colloid densities and substrate molarities. In total, results from thirteen experiments are presented here, covering six different substrate molarities (Table II).

A typical sample of images acquired during the aggregation process is shown in Fig. 1. The colloidal monolayers were found to be somewhat mobile, due to air currents, convection, etc. The pictures do not, therefore, represent the evolution of a unique part of the colloidal monolayer, but rather are quasirandomly selected samples. This should not affect the conclusions drawn below as the self-similarity of structures developing in random aggregation processes is statistical in nature.

Superimposed on such overall drifts, individual particles and clusters could be seen to exhibit random saltatory motions. While we have no definitive proof of the Brownian nature of these motions, their random character will clearly influence the aggregation process. Thus it should be appropriate to compare the present experimental results with predictions for diffusion-limited cluster-cluster aggregation, and its reaction limited variant.

The influence of potential artifacts upon the results was carefully considered: only one possible problem was found. The distribution $P(\theta)$ of the orientation of the clusters relative to the long axis of the digitized pictures was found to be nonuniform in all experiments analyzed, being enhanced in the intervals 10°–20° and 160°–170°. Further analysis showed that the cluster size and orientation were highly correlated for $s \lesssim 15$ pixels [Fig. 2(a).] This arises from the discrete set of orientations possible for the digitized images of such small clusters. For example, only 21 distinct arrangements of 4 pixels are possible, and the observed nonuniform $P(s, \theta)$ can be reproduced provided that these various arrangements are not equally probable. Similar problems were evident in the distribution of cluster anisotropy [Fig. 2(b)] where correlations between s and A' were evident for clusters of 4 pixels. These problems led us to exclude such small clusters ($s \leq 4$) from all the analyses.

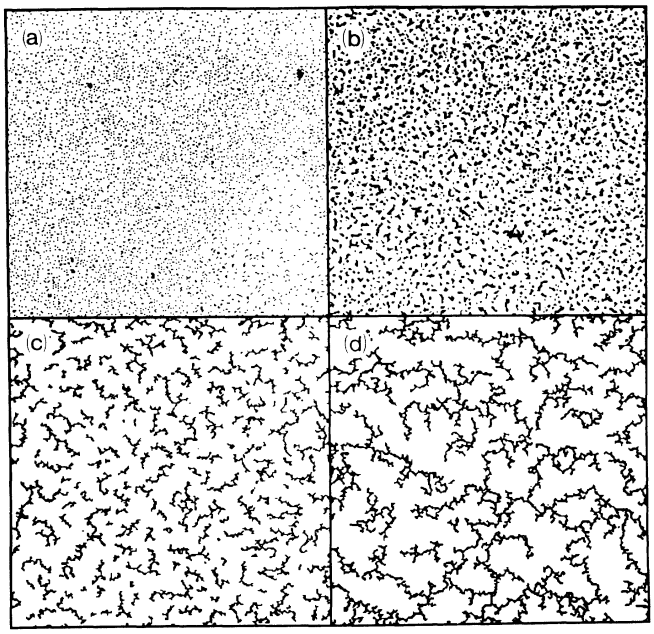

FIG. 1. Four pictures at different stages of aggregation of a colloidal monolayer on a 0.73M $CaCl_2$ substrate. Times after initiation of aggregation: (a) 15, (b) 75, (c) 105, (d) 135 min. Each picture represents the center 512 × 512 pixel section from a 768 × 512 image.

A. Fractal dimension

For each method used to determine the fractal dimensions of the colloidal aggregates, clusters from all images observed throughout an experiment were incorporated in a single analysis to ensure as good statistics as possible. This involves the implicit assumption that the scale-invariant character of the clusters does not change systematically as the aggregation proceeds. The goal of good statistics was achieved: between 11 000 and 51 000 clusters were analyzed per experiment.

1. Radius of gyration method

Figure 3 shows a typical double-logarithmic plot of s (here the average cluster size) vs R_g^2. The scale invariance of the clusters is evident over nearly two orders of

magnitude of s.

The line shown represents the best-fit linear variation to all but the three lowest points, which evidently depart from the asymptotic scale invariance of the larger clusters. In the data fitting the points were weighted by the number of clusters contributing to them. The fractal dimension of the clusters in this experiment was 1.540 ± 0.008, in accord with that characteristic of two-dimensional RLCA. The value of D found was largely independent of the range of s over which the fit was performed. In this respect our results differ from certain previous reports [28, 30]. These differences may derive from the excellent statistics of the present experiment, as well as the direct noninvasive imaging techniques used. The direct acquisition of digitized images, coupled with semi-automatic image analysis permitted very large numbers of aggregates to be analyzed, giving confidence in the fitted values of D. The residuals of the fit shown were small (typical deviation in $\log_{10} s < 0.1$) and uncorrelated, as in all our experiments.

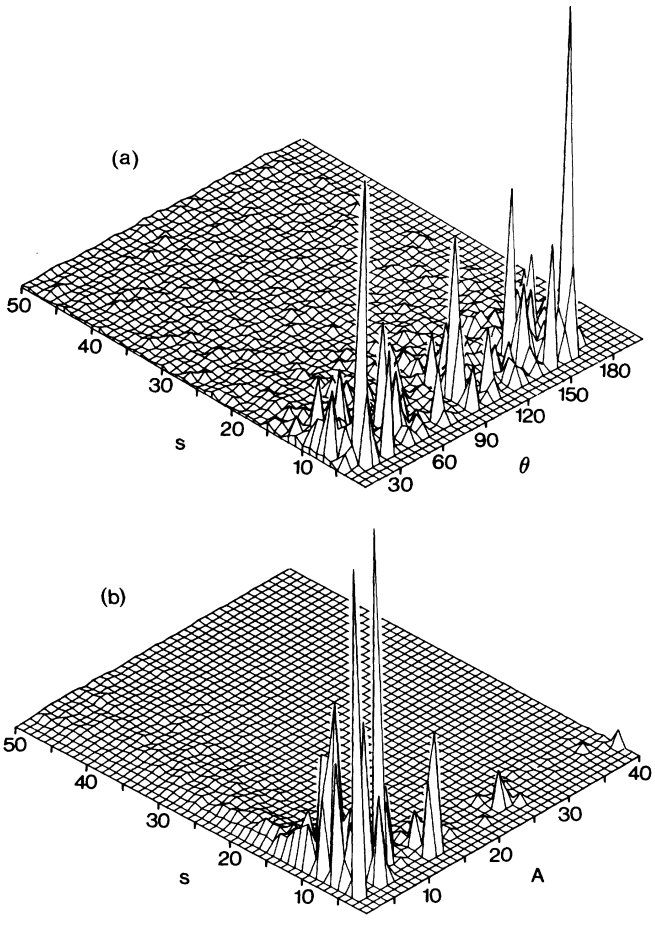

FIG. 2. Distributions of (a) the orientation (θ) of the largest principal axis of the clusters with respect to the length of the video images and (b) the anisotropy as functions of the clusters of size n. The distributions represent all clusters with $1 < s < 50$ pixels observed in all experiments involving $0.73M$ $CaCl_2$ substrates (1.73×10^5 clusters in all).

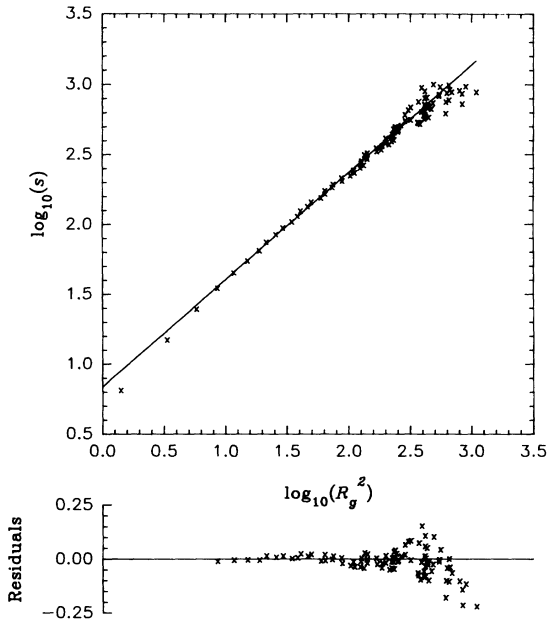

FIG. 3. Plot of $\log_{10} s$ vs $\log_{10} R_g^2$ for an experiment with a $0.36M$ $CaCl_2$ substrate. Each point represents s and R_g^2 averaged over a range of 10 in s. The graph includes data for 1.9×10^4 clusters at all stages of growth, reflecting about 8.35×10^5 pixels (and hence particles) in total. The line is the best-fit linear variation, of slope $\frac{1}{2}D = 0.770 \pm 0.004$. The residuals of the fit are consistent with zero.

For the lowest three points of Fig. 3 the gradient of the graph was 1.90 ± 0.02. There is thus a change in the scaling behavior at $s \sim 25$ pixels, smaller clusters being more compact than the larger ones. It seems likely that in RLCA small clusters would be more compact, as the sticking probability would be greater at "interior" corners of clusters. There may also be effects due to short-range interactions or from restructuring of the clusters, which could result in substantially more compact structures at small length scales [32].

Data for the other experiments at different substrate concentrations were similarly analyzed, D being extracted using data over a range of $40 < s < 800$. However, in those cases where larger clusters were observed, as in Fig. 3, the corresponding points fitted rather well onto the lines fitted to the data over this range. The resulting values of D are summarized in Table II, and will be discussed below.

2. *Nested-squares method*

Figure 4 shows a double-logarithmic plot of $N_b(l)$ vs l, the data being averaged over all clusters observed in the experiment. Equation (3) enabled the fractal dimension to be determined, the data being weighted by the relative uncertainty in $N_b(l)$, assumed to be $N_b^{-1/2}$. As for the radius of gyration method, the three points at lowest l were omitted from the fits, as on small scales the clusters seemed more compact. These points involved

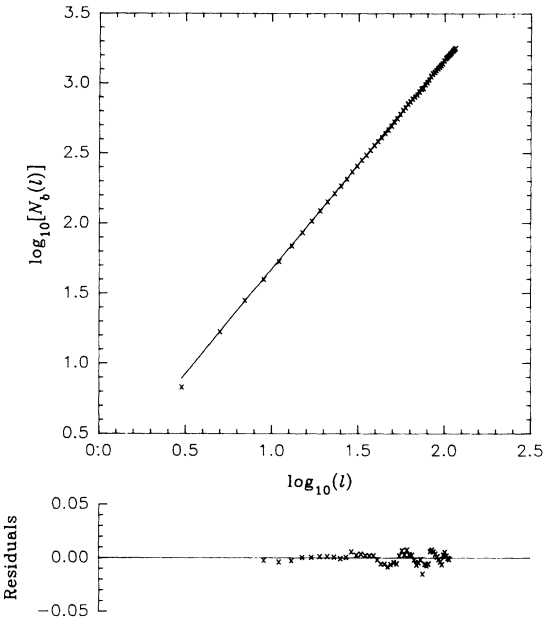

FIG. 4. A log-log plot of $N_b(l)$ vs l, for $3 < l < 120$, on a $0.73M$ $CaCl_2$ substrate. The straight-line fit has gradient $D = 1.461 \pm 0.007$. Note the residuals, which are much smaller than in Fig. 3.

$l = 3$–9 pixels, corresponding to the range of cluster sizes omitted from the radius of gyration method. Any values of $N_b(l)$ averaged over less than four clusters were also omitted, to avoid the effects of poor statistics.

The graphs were much less noisy than those for the radius of gyration method, because here a given cluster contributes to all points up to l equal to the cluster size, whereas it would contribute to only one point in the previous method. The values of the fractal dimension found from the nested-squares method were thus more precise than the previous results. The residuals of the linear fits to the plots were always consistent with being randomly distributed about zero. Fluctuations of the residuals at large l were consistent with those found in tests on polydisperse samples of deterministic images, and are not significant.

The results from the nested-squares algorithm are summarized in Table II, and within the errors agree well with those from the radius of gyration method.

3. *Direct correlation function*

Cluster-cluster aggregation leads to anisotropic clusters. However, the density correlations *within* the clusters remain isotropic. Thus the assumption, implicit in the correlation function method, that a pixel within a cluster is equally likely to be found in all directions will be satisfied adequately by averaging over many clusters randomly oriented in space. The isotropy of $P(s, \theta)$ for $s \geq 15$ pixels (Fig. 2) indicates that this requirement was met in the present experiments.

A typical correlation function computed for clusters of $s \geq 30$ is shown in Fig. 5. The function displays three types of behavior, reflecting the fact that random fractals are only self-similar over a limited range of length scales. The slow decay of $C(r)$ at small r indicates the relatively compact nature of the central region of the clusters noted above. At large r the correlations vanish due to the finite extent of the clusters. The average cluster size, estimated from the average number of pixels within the clusters and the scaling of Eq. (3), coincided reasonably well with the apparent disappearance of fractal scaling of $C(r)$. Between these limits $C(r)$ decayed with a slope $\alpha = D - d$. Unfortunately the range over which $C(r)$ exhibited this self-similarity was rather limited, so that estimates of D were rather less accurate than for the previous two methods. Values of D found over the range of substrate concentration are summarized in Table II, and essentially agree with those from the other methods.

B. Cluster anisotropy

The anisotropy of the clusters observed in this work is apparent in Fig. 1, and was quantitatively investigated. The measure used was the average of the ratio of the principal radii of gyration of the clusters (A'). This avoids evident problems associated with averaging the individual radii of gyration over a set of clusters varying widely in size.

Scaling arguments [31] suggest that the anisotropy should be almost independent of cluster size: $A(s) \propto A(\infty) + C(R_g^{-2})$, where the size-dependent term is about

TABLE II. Summary of measured parameters. Where more than one experiment was performed at a given molarity the values quoted are the weighted means of the figures from the individual experiments.

Conc. $CaCl_2$ (M)	No. expts.	D (R_g)	D (squares)	D [$C(r)$]	A'
0.25	1	1.576 ± 0.015	1.577 ± 0.007	1.60 ± 0.05	3.90 ± 0.21
0.36	1	1.540 ± 0.008	1.554 ± 0.006	1.50 ± 0.07	5.45 ± 1.19
0.45	2	1.548 ± 0.016	1.555 ± 0.007	1.63 ± 0.06	4.61 ± 0.47
0.55	1	1.412 ± 0.012	1.452 ± 0.009	1.43 ± 0.04	5.15 ± 0.47
0.73	6	1.448 ± 0.005	1.450 ± 0.002	1.44 ± 0.01	5.75 ± 0.23
0.91	1	1.441 ± 0.019	1.453 ± 0.014	1.38 ± 0.08	6.13 ± 1.42

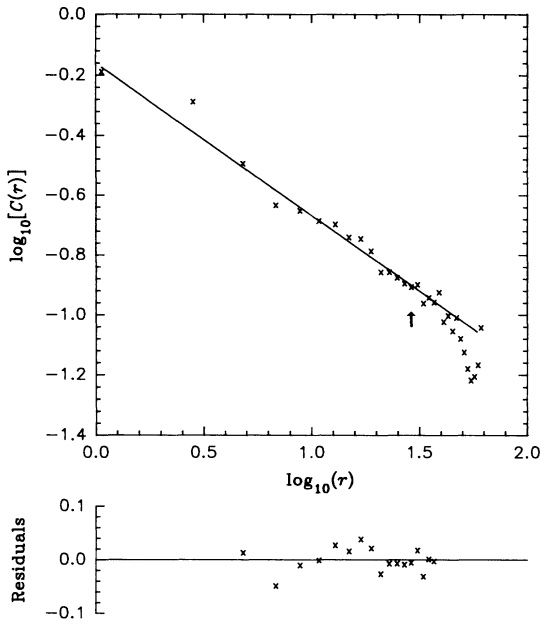

FIG. 5. Plot of $\log_{10} C(r)$ vs $\log_{10} r$ for an experiment on a $0.55M$ $CaCl_2$ substrate. The arrow indicates the approximate average cluster size ($\log_{10} \bar{r} = 1.38$), computed as detailed in the text. The line is a linear fit to the data over a range $5 < r < 38$. The slope $\alpha = -0.57 \pm 0.04$ yields an estimate of $D = 1.43$.

two orders of magnitude smaller than the asymptotic function $A(\infty)$. In fact, the anisotropy evaluated for all clusters in all six experiments for the $0.73M$ $CaCl_2$ subphase showed no systematic change with time (measured from the injection of the electrolyte into the subphase) as the aggregation proceeded (Fig. 6). While the data were rather scattered, they tended to confirm the theoretical suggestions, so we feel justified in averaging the measured values of anisotropy found for all images in an experiment under given physical conditions.

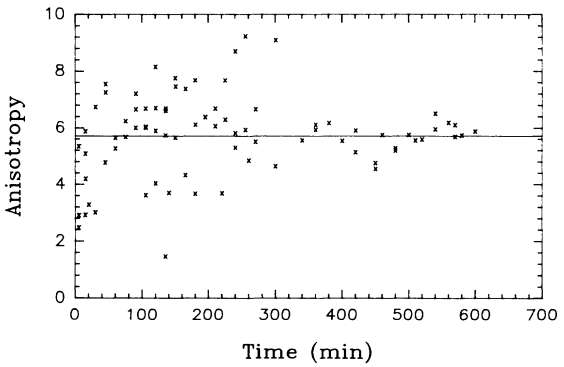

FIG. 6. The time variation of the cluster anisotropy. Each point represents an average over all clusters in an image, the data representing all images in all experiments for $0.73M$ $CaCl_2$ substrates. Over the range of t shown the average cluster size rose from ~ 32 to ~ 360.

The values for the anisotropy for the various substrate concentrations are shown in Table II. While the quantitative differences are not large compared to the errors, the measured values appear to increase systematically with increasing substrate molarity.

V. DISCUSSION

The fractal dimension of the colloidal aggregates as measured by all methods are summarized in Table II. The aggregates appear to be self-similar over the entire accessible range of length scales, no deviations being apparent. Within errors the results from all three methods concur. There is, therefore, no need to treat the three sets of results separately. We consider only the most precise, those from the nested-squares method.

For one substrate concentration ($0.73M$) six experiments were performed, spanning a range of surface concentration of colloidal particles in excess of two: the fitted values of fractal dimension (ranging from 1.425 ± 0.006 to 1.465 ± 0.004) did not vary significantly, indicating the absence of any effects due to surface density. This set of experiments also embraced some variation in the procedure used to poison the substrate with $CaCl_2$: the constancy of D indicates that the only major factor governing the fractal structure of the aggregates was the final concentration of counterions in the subphase.

The cluster self-similarity extended over the entire range of length scales examined, apart from some departures at small scales due to some restructuring or other effects. The residuals of the fits to the data were small and uncorrelated, and demonstrate the adequacy of the power-law scaling implicit in the fits over the entire range of lengths probed. In contrast to certain previous studies involving imaging of three-dimensional aggregates [28,30] there was no need to invoke any more complicated form of scaling behavior than the fractal self-similarity embodied in Eq. (3). The absence of exponential correction terms due to cluster edge effects in the present data is due to the excellent statistics, as well as the absence of projection effects for our two-dimensional clusters.

The variation of D with substrate molarity is shown in Fig. 7. The data clearly fall into two classes, lying above and below a substrate molarity of about $0.5M$. The values determined for D in the two regimes are compatible with predictions for the DLCA and RLCA processes (cf. Table I). As might have been expected, at low counterion concentrations RLCA apparently occurs, whereas at the high concentrations DLCA is observed. The nature of the crossover from RLCA to DLCA is not yet completely understood [27]: simulations tend to suggest a continuous transition from one regime to the other, whereas theoretical considerations imply a sudden jump, depending on the exponents of scaling of the sticking probability [33] and of the diffusion constant of the clusters [34]. Experimentally there appears to be a step change in D as the concentration of the $CaCl_2$ subphase is increased. The data are consistent with a sudden change from one aggregation mechanism to the other, although a transition extending over a small range of the $CaCl_2$ concentration

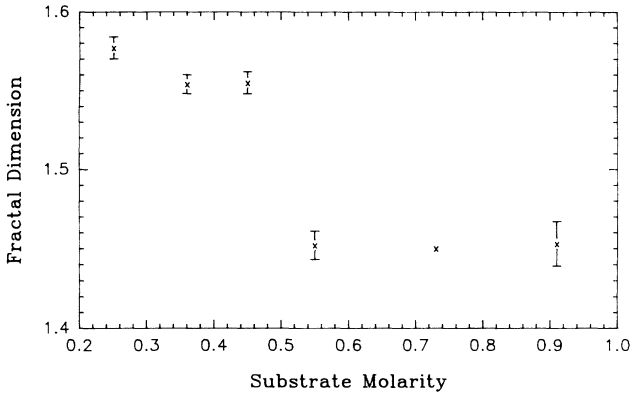

FIG. 7. The fractal dimension, determined by the nested-squares method, for experiments on substrates of different $CaCl_2$ molarities.

between $0.45M$ and $0.55M$ cannot be ruled out.

Turning to the anisotropies (Fig. 8), the first point to be made is that the measured values do not seem constant, but rather increase with the subphase molarity. The probability that the data are constant, equal to the overall weighted mean (4.79 ± 0.14), is $\ll 1\%$. The anisotropies may simply increase with subphase molarity, as expected for finite systems. However, it seems reasonable to separate the results into two groups on the basis of the fractal dimension. The weighted mean anisotropies found for these two groups are 4.05 ± 0.19 for low concentrations and 5.64 ± 0.20 for high ones. While the quantity measured corresponded to the definition of A', these average values are actually in reasonable agreement with the values of A quoted in Table I: the probability (from χ^2) that the measured anisotropies are consistent with these values is $\sim 15\%$, which is perfectly acceptable. The data are in very much poorer agreement with the theoretical values of A'.

The exact reason for this discrepancy is not entirely clear, but it may not be entirely surprising in view of the simplicity of the theoretical models used: these models do not, and probably cannot, incorporate all physical

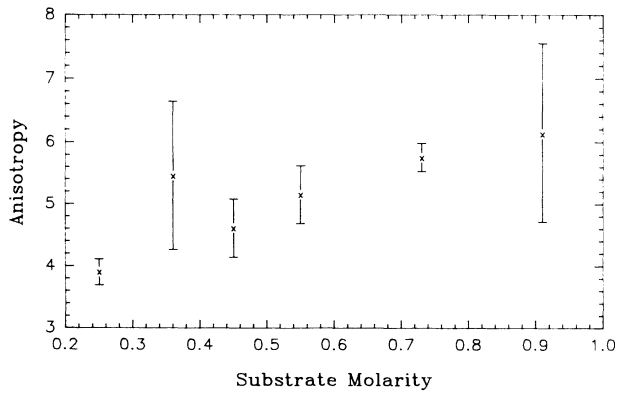

FIG. 8. The dependence of the cluster anisotropy upon substrate molarity.

processes which must be present in an experimental system. To cite only one example, hydrodynamic effects could lead to indirect cluster-cluster interactions via the fluid.

Slight changes in the model used in computer simulations can lead to observable differences in the statistical structure of the aggregates formed. For example, cluster polarizability may lead to a tip-to-tip tendency in the aggregation [22], which would clearly increase the anisotropy, but also leads to a considerable reduction in the fractal dimension (to 1.28). Again, many cluster-cluster simulations involve a growth process in which only clusters of specified size are present at any one time. The computed values of the anisotropy derive from the so-called hierarchical model of cluster-cluster aggregation [35], in which all clusters at any time are of unique size, it being argued that the radii of gyration (hence D and A) should not be affected by this simplification. However, it has been shown that including cluster polydispersity in the model causes a significant increase in the fractal dimension of the clusters (from 1.53 to 1.59 in two dimensions), presumably due to the possibility of penetration of the larger clusters by smaller ones. It is not clear what effect polydispersity would have on A, but it could be significant.

It is thus premature to attempt to draw definite conclusions from our measured values of D and anisotropy, as minor changes in modeling the aggregation process can cause appreciable differences in the predictions. We can, however, conclude that the anisotropy does carry extra information, separate from, and complementary to the fractal dimension.

The two previous studies of fractal aggregation of colloidal particles trapped at a liquid surface seem to have differed somewhat from the present work. For a gelled surface after the sol-gel transition [17] a crossover was observed from DLCA-like structure ($D = 1.42$) over short lengths ($\lesssim 30$ particles) to a much more compact, gelled structure ($D = 1.69$) over larger distances. Large clusters found in regions of the surface not invaded by the gel seemed much less compact ($D \sim 1.20$), although averaged over all clusters $D \sim 1.6$ in such regions. Another study [16] found $D \sim 1.2$ for length scales greater than about 10 particle radii, the data apparently being taken just before gelation occurred. In the only other experimental study of cluster structure as a function of growth conditions, the variation of D with growth rate was determined for colloidal particles suspended between solid walls [18]. Excess electrolyte only seems to have been used to achieve the very highest growth rates, for which D appeared to approach the diffusion limited aggregation value of 1.67 (for particle-cluster aggregation). Again, this may have been due to a sol-gel transition. Further discussion of differences from the present results would seem mere speculation in view of the various experimental differences.

The induction of aggregation, and particularly the transition to a regime of apparent DLCA, required large concentrations of $CaCl_2$ in the aqueous subphase. Such concentrations were also found to be necessary in a pre-

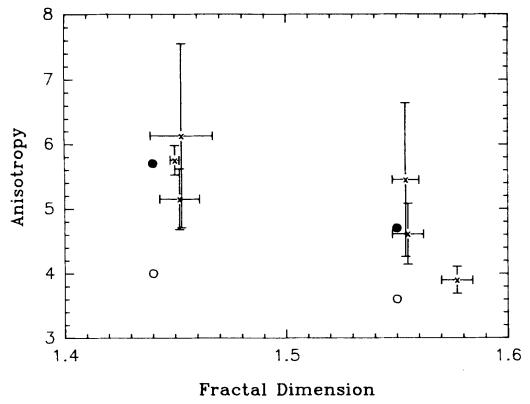

FIG. 9. Plot of fractal dimension (from the nested-squares method) vs cluster anisotropy. The crosses represent measured values (see Table II), the circles theoretical predictions [using A (•) and A' (○)].

vious study of surface colloidal aggregation [16]: it was suggested that the ionic density near the surface is substantially less than in the bulk fluid, due to electrostatic effects. A more detailed discussion is deferred until paper III, where the aggregation mechanism will be considered in depth.

The present results are summarized in Fig. 9. This plot of the measured anisotropies against fractal dimension for the several experiments at different substrate molarities clearly shows how the data separate into two groups. Each group is scattered about the expectation value for either DLCA or RLCA: within the experimental errors we can conclude that the structures formed by cluster-cluster aggregation appear to fall into one or other of these two categories. The change from one regime to the other appears to be governed only by the substrate molarity. We note that there seems no gradual progression between the two extremes, but rather a comparatively sudden transition. Any transitional variation would have to span a narrower range than from $0.45M$ to $0.55M$.

VI. CONCLUSIONS

We have measured the morphological characteristics of structures formed in colloidal particle monolayers aggregating in the presence of electrolyte, subject to the influences of Brownian motion, electrostatic, and capillary forces. Other influences may well have been present, but are not so readily identifiable. Over the range of length scales accessible to experimental observation, the clusters formed display statistical self-similarity. The measured values of the fractal dimension and cluster anisotropy are in good accord with expectation from computer simulation. Certain minor discrepancies can be ascribed to the simplicity of current computer simulations.

ACKNOWLEDGMENTS

This work was supported by the SERC. One of us (D.J.R.) gratefully acknowledges financial support from DENI and Unilever Research.

[1] M. Kolb and R. Jullien, J. Phys. (Paris) Lett. **45**, L977 (1984).
[2] P. Meakin, Phys. Rev. Lett. **51**, 1119 (1983).
[3] P. Meakin, in *Phase Transitions and Critical Phenomena*, edited by C. Domb and J.L. Lebowitz (Academic, New York, 1988), Vol. 12, p. 335.
[4] R. Botet, R. Jullien, and M. Kolb, J. Phys. A **17**, L75 (1984).
[5] M.Y. Lin, H.M. Lindsay, D.A. Weitz, R.C. Ball, R. Klein, and P. Meakin, Proc. R. Soc. London Ser. A **423**, 71 (1989).
[6] D.A. Weitz and M.Y. Lin, Phys. Rev. Lett. **57**, 2037 (1986).
[7] D.J. Robinson and J.C. Earnshaw, following paper, Phys. Rev. A **46**, 2055 (1992).
[8] D.J. Robinson and J.C. Earnshaw, this issue, Phys. Rev. A **46**, 2065 (1992).
[9] P. Pieranski, Phys. Rev. Lett. **45**, 569 (1980).
[10] J.C. Earnshaw, J. Phys. D **19**, 1863 (1986).
[11] B. LeNormand, Physica D **38**, 230 (1989)
[12] W.J. Popiel, *Introduction to Colloid Science* (Exposition, Hicksville, NY, 1978).
[13] E. Dickinson, Colloids Surf. **42**, 191 (1989).
[14] C. Camoin and R. Blanc, J. Phys. (Paris) Lett. **46**, L67 (1985).
[15] P. Richetti, J. Prost, and P. Barois, J. Phys. (Paris) Lett. **45**, L1137 (1984).
[16] A.J. Hurd and D.W. Schaefer, Phys. Rev. Lett. **54**, 1043 (1985).
[17] A.J. Armstrong, R.C. Mockler, and W.J. O'Sullivan, J. Phys. A **19**, L123 (1986).
[18] A.T. Skjeltorp, Phys. Rev. Lett. **58**, 1444 (1987).
[19] G. Helgesen, A.T. Skjeltorp, P.M. Mors, R. Botet, and R. Jullien, Phys. Rev. Lett. **61**, 1736 (1988).
[20] C. Allain and B. Jouhier, J. Phys. (Paris) Lett. **44**, L421 (1983).
[21] H.J. Herrmann and M. Kolb, J. Phys. A **19**, L1027 (1986).
[22] R. Jullien, J. Phys. A **19**, 2129 (1986).
[23] J.C. Earnshaw and D.J. Robinson, Prog. Colloid Polym. Sci. **79**, 162 (1989).
[24] D.Y.C. Chan, J.D. Henry, and L.R. White, J. Colloid Interface Sci. **79**, 410 (1981).
[25] A.J. Hurd, J. Phys. A **18**, L1055 (1985).
[26] H. Takayasu, *Fractals in the Physical Sciences* (Manchester University Press, Manchester, 1990), p. 11.
[27] T. Vicsek, *Fractal Growth Phenomena* (World Scientific, Singapore, 1989), p. 80, p. 216.
[28] M. Tence, J.P. Chevalier, and R. Jullien, J. Phys. (Paris) **47**, 1989 (1986).

[29] R. Jullien and R. Botet, *Aggregation and Fractal Aggregates* (World Scientific, Singapore, 1987), p. 88.
[30] S.R. Forrest and T.A. Witten, J. Phys. A **12**, L109 (1979).
[31] R. Botet and R. Jullien, J. Phys. A **19**, L907 (1986).
[32] P. Meakin and R. Jullien, J. Phys. (Paris) **46**, 1543 (1985).
[33] F. Family, P. Meakin, and T. Vicsek, J. Chem. Phys. **83**, 4144 (1985).
[34] P. Meakin, F. Vicsek, and T. Family, Phys. Rev. B **31**, 564 (1985).
[35] R. Jullien and M. Kolb, J. Phys. A **17**, L639 (1984).

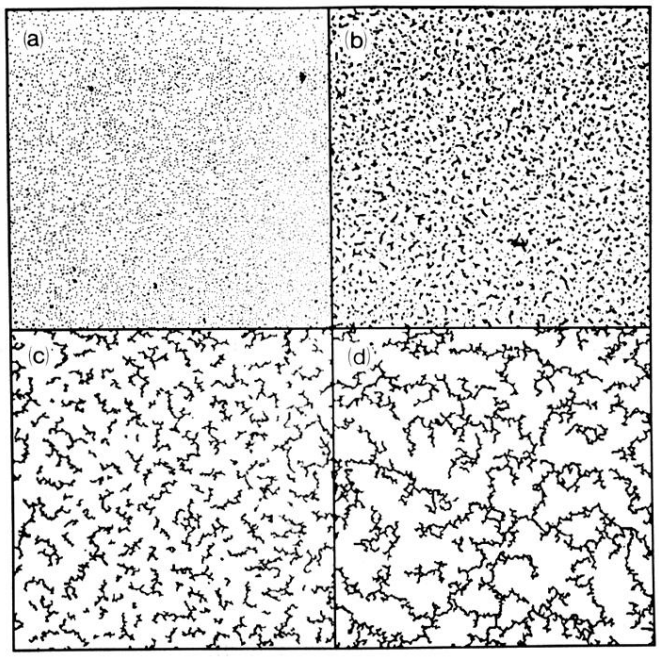

FIG. 1. Four pictures at different stages of aggregation of a colloidal monolayer on a 0.73M $CaCl_2$ substrate. Times after initiation of aggregation: (a) 15, (b) 75, (c) 105, (d) 135 min. Each picture represents the center 512×512 pixel section from a 768×512 image.